



**HAL**  
open science

# Doping-driven resistive collapse of the Mott insulator in a minimal model for VO<sub>2</sub>

L Fratino, S Bag, A Camjayi, M Civelli, M Rozenberg

► **To cite this version:**

L Fratino, S Bag, A Camjayi, M Civelli, M Rozenberg. Doping-driven resistive collapse of the Mott insulator in a minimal model for VO<sub>2</sub>. *Physical Review B*, 2022, 105 (12), pp.125140. 10.1103/physrevb.105.125140 . hal-03854088


**HAL Id: hal-03854088**

**<https://hal.science/hal-03854088v1>**

Submitted on 15 Nov 2022

**HAL** is a multi-disciplinary open access archive for the deposit and dissemination of scientific research documents, whether they are published or not. The documents may come from teaching and research institutions in France or abroad, or from public or private research centers.

L'archive ouverte pluridisciplinaire **HAL**, est destinée au dépôt et à la diffusion de documents scientifiques de niveau recherche, publiés ou non, émanant des établissements d'enseignement et de recherche français ou étrangers, des laboratoires publics ou privés.

**Doping-driven resistive collapse of the Mott insulator in a minimal model for VO<sub>2</sub>**L. Fratino<sup>1</sup>, S. Bag<sup>1</sup>, A. Camjayi,<sup>2</sup> M. Civelli,<sup>1</sup> and M. Rozenberg<sup>1</sup><sup>1</sup>*Université Paris-Saclay, Centre National de la Recherche Scientifique Laboratoire de Physique des Solides, 91405 Orsay, France*<sup>2</sup>*Universidad de Buenos Aires, Ciclo Básico Común and CONICET, Universidad de Buenos Aires, Instituto de Física de Buenos Aires, Pabellón 1, Ciudad Universitaria, 1428, CABA, Argentina* (Received 13 September 2021; revised 9 March 2022; accepted 10 March 2022; published 30 March 2022)

We study the resistive collapse of the Mott insulator state in the dimer Hubbard model. This minimal model has been used to describe the physics of VO<sub>2</sub>, and should be relevant to other strongly correlated materials. It incorporates the physics of correlated dimers and the explicit competition between on-site Coulomb repulsion and magnetic exchange interactions. Our results unveil that between the Mott insulator at half filling and the Fermi liquid metal at high doping there is an intermediate bad metallic phase with exotic features such as a pseudogap, orbital selectivity, and a first-order metal-metal transition. The model is solved within dynamical mean field theory by means of quantum Monte Carlo, which provides the numerically exact solution of the model in the limit of large lattice dimensionality. This model can be considered as a minimal one that captures exotic phenomena associated to the physics of a doped Mott insulator, shading light on their basic physical mechanism.

DOI: [10.1103/PhysRevB.105.125140](https://doi.org/10.1103/PhysRevB.105.125140)

Strongly correlated transition metal oxides have remained at centerstage of condensed matter physics for almost 40 years now [1]. Their interest has been motivated by an endless stream of fascinating and diverse experimental discoveries. The highlights range from high temperature superconductivity in cuprates since the 1980s [2], to colossal magnetoresistance in manganites in the 1990s [3], to neuromorphic functionalities in vanadates and nickelates in the 2010s [4].

The key unifying concept is that all that exotic physics emerges upon doping a Mott insulator state. The Mott materials are peculiar because they are expected to have partially filled bands and therefore metals, however, due to strong electronic correlations, turn out to be insulators [5]. Despite great theoretical efforts and the development of powerful numerical techniques, the understanding of the physics of states emerging from doped Mott insulators remains one of the most challenging and relevant problems of condensed matter physics.

A Mott insulator of great current interest is VO<sub>2</sub>, which has an insulator to metal Mott transition (IMT) near room temperature, at about 340 K; thus, it may have multiple practical applications [6]. Interestingly, the Mott insulator phase of VO<sub>2</sub> is monoclinic, where pairs of V atoms are dimerized. It was recently shown that the dimer Hubbard model (DHM), which is an extension of the Hubbard model where each unit cell contains a dimer, is useful to interpret experiments in VO<sub>2</sub> across the IMT [7–9]. However, doping the VO<sub>2</sub> Mott insulator by chemical substitution turns out to be difficult, with relatively few reports available [10,11]. Thus, other exciting possibilities are currently pursued. Some prominent examples are electrostatic doping [12,13] and electronic injection [14]. The ability to induce the resistive breakdown of the Mott state by electric fields may open new roads into so-called neuro-

morphic functionalities, such as artificial neuron electronic devices [4,15–17]. The insulator and metallic electronic states of VO<sub>2</sub> have also been intensively studied within realistic dynamical mean field theory (DMFT) [18–21]. Interestingly, the impurity problem in that approach is a multiorbital version of the DHM. Thus, the understanding of the doping-driven collapse of the Mott insulator state in the DHM within DMFT is a relevant problem to solve, as a first approximation to the physics of the IMT in VO<sub>2</sub>.

The DHM is also of fundamental interest from a different perspective. It is arguably the simplest many-body model of Mott insulators that explicitly has a competition between local Coulomb repulsion and magnetic exchange interactions. While in the absence of carriers doping this competition is naturally resolved by an antiferromagnetic Mott insulator, the fate of the state upon doping remains a challenge and is considered to be at the root of the rich variety of exotic phenomena found in correlated transition metal oxides. This prominently includes, in the context of unconventional superconductors, the ongoing debate on the existence of a paradigmatic quantum phase transition between two metals that is characterized by the absence of any broken symmetry, in sharp contrast with the conventional scenario [22,23].

Here, we shall focus our efforts on the doping-driven collapse of the Mott state in the DHM. Fortunately, this problem can be treated within DMFT by means of numerical methods that provide essentially the exact solution [24–26]. The DMFT has already proven a successful approach in the investigation of the Mott transition in the Hubbard model, providing insights on the physics of another famous Mott vanadate, V<sub>2</sub>O<sub>3</sub> [27]. Interestingly, the doping-driven transition in the DHM is qualitatively different. Among the main results of our paper we shall show that the Mott insulator evolves first into an

unconventional bad metal phase [that we call the pseudogap (PG) metal] and then into a Fermi (FL) liquid one [26,28–34]. One particularly unexpected feature of the exotic state is that it can be described as a semimetallic orbital-selective Mott state [25,35–40]. We find that the optical response of this bad metal state has a tiny Drude component, which may possibly be observed in optical conductivity experiments.

Akin to the above-mentioned Mott transition in the Hubbard model, our results suggest that the PG-metal-to-metal transition in the DHM may have universal character, thus potentially relevant to many correlated quantum materials. In fact, many unconventional properties that received continuous attention are naturally realized in the solution of the DHM, such as a pseudogap state, metallicity without quasiparticles, enhanced compressibility, and orbital selectivity. Thus, we may argue that the doping-driven IMT in the simultaneous presence of Coulomb repulsion and magnetic exchange may be the long-sought phenomenon where many exotic quantum states are originated [41].

## I. MODEL AND METHOD

The DHM consists of a lattice of dimers:

$$\mathcal{H} = \sum_{i,j;\sigma=\uparrow,\downarrow} \psi_{i,\sigma}^\dagger \mathbf{T}_{i,j} \psi_{j,\sigma} + U \sum_{i;\alpha=1,2} n_{i\alpha\uparrow} n_{i\alpha\downarrow}. \quad (1)$$

The spinor  $\psi_{i,\sigma} = (c_{i,1,\sigma}, c_{i,2,\sigma})$  acts on the dimer sites  $\alpha = 1, 2$  at the lattice site  $i$ , with  $c_{i\alpha\sigma}^\dagger$  and  $c_{i\alpha\sigma}$  the electron creation and destruction operators, respectively. The matrices  $\mathbf{T}_{i,j} = -t\hat{1}$  and  $\mathbf{T}_{i,i} = -\mu\hat{1} + t_\perp\hat{\sigma}_x$  ( $\hat{\sigma}_x$  is the first Pauli matrix) describe the nearest-neighbor interdimer and the intradimer electron hopping, respectively. Electrons experience strong correlation via the on-site local repulsion  $U$ . We adopt  $t = 0.5$  and  $t_\perp = -0.3$ , and fix the on-site local repulsion term  $U = 2.3$  in order to be deep in the correlated regime. A similar set of parameters has been used in the study of the model at half filling, where it exhibits a first-order temperature-driven insulator-to-metal transition [8,42]. The small difference is due to the previous study being done with iterated perturbation theory, while the present one is with quantum Monte Carlo (QMC). Here, we shall also vary the chemical potential  $\mu$  to induce a doping-driven insulator-to-metal transition by adding or removing electrons.

The advantage of the DHM is that in the infinite dimensional limit DMFT provides the exact solution [8,42–47]. We can then establish properties of the doped metallic state and its possible phase transitions without the uncertainty introduced by an approximation, such as in the cluster DMFT treatments of the two-dimensional Hubbard model on a square lattice. It is convenient to express the DMFT equations in the diagonal bonding/antibonding ( $B/AB$ ) basis of the lattice hopping matrix  $\mathbf{T}_{i,j}$ . The dimer Green's function in the  $B/AB$  basis can be written in terms of the components of the site basis Green's function  $G_{\alpha\beta}$  as  $\text{diag}(G_B, G_{AB}) = \text{diag}(G_{11} - G_{12}, G_{11} + G_{12})$ , where we dropped the spin indices for clarity. In the infinite dimensional limit, adopting a semicircular (i.e., Bethe lattice) density of states  $D(\epsilon) = -\frac{1}{t\pi} \sqrt{[1 - (\frac{\epsilon}{2t})^2]}$ , the DMFT self-consistency equations are then readily written:

$$\mathcal{G}_{oB/AB}^{-1}(\omega_n) = i\omega_n + \mu \pm t_\perp - t^2 G_{B/AB}(\omega_n) \quad (2)$$

where  $\mathcal{G}_{oB/AB}(\omega_n)$  is the Weiss field describing the bath of the dimer Anderson impurity model (DAIM) associated to the Hamiltonian (1). We solve the DAIM imaginary-time action

$$S_{\text{DAIM}} = - \int_0^\beta d\tau d\tau' \sum_{\substack{\sigma=\uparrow,\downarrow \\ \alpha,\beta=1,2}} c_{\alpha\sigma}^\dagger(\tau) \mathcal{G}_{o\alpha\sigma,\beta\sigma}^{-1}(\tau - \tau') c_{\beta\sigma}(\tau') \\ + U \int_0^\beta d\tau \sum_{\alpha=1,2} n_{\alpha\uparrow}(\tau) n_{\alpha\downarrow}(\tau) \quad (3)$$

using continuous time quantum Monte Carlo (CTQMC) within the hybridization expansion approach [48,49]. The self-consistent determination of Eqs. (2) and (3) outputs  $G_{B/AB}(\omega_n)$  and the respective self-energies, which embody all the physical information that we need. On the technical side, for simplicity, Eq. (3) is expressed in the site basis. The eigenstates of the isolated dimer Hamiltonian in the two bases are given in Table I, where

$$s = \sin(\theta), \quad c = \cos(\theta)$$

and

$$\theta = \arctan \left( \frac{-U}{4t_\perp + \sqrt{16t_\perp^2 + U^2}} \right)$$

and

$$\sigma_{1/2} = \frac{4t_\perp}{\mp U + \sqrt{U^2 + 16t_\perp^2}}.$$

## II. RESULTS

Our main result is shown in Fig. 1, where we display the total density  $n$  as a function of the chemical potential  $U/2 - \mu$ , shifted with respect to the half-filled case. As previously reported [8,42], for  $\mu = U/2$  the system is in a Mott insulator. This can be right away seen by following the  $n$  vs  $U - \mu/2$  behavior at the lowest temperatures  $T$ . It displays the horizontal plateau of electronic incompressibility at half filling  $n = 2$ , which is the hallmark of a Mott insulating state. By varying  $\mu$ , we can dope particles and holes so to drive a transition to a metallic state. Here we consider the hole-doping case, i.e.,  $n < 2$  (note that data would be symmetric for particle doping). At high temperatures, the system can be considered a poor metal or semiconductor as we see that there is a finite slope at the origin of the  $n$  vs  $\mu$  curve at  $\beta = 25$ . This indicates that there is a finite compressibility. At lower  $T$  we see that the  $n$  vs  $\mu$  is flat at the origin, which is a signature of the incompressible Mott insulator state. Upon increasing  $U/2 - \mu$ , i.e., doping the system, we observe an *enhancement* of the compressibility ( $\propto dn/d\mu$ ) at low  $2 - n$ . This can be seen already at  $\beta = 32$ . At lower  $T$  the behavior becomes more remarkable as both the plateau becomes wider and the compressibility enhancement becomes stronger. At  $\beta = 50$ , we can observe that around  $U/2 - \mu \simeq 0.23$  the system is already deep in a metallic and high compressible state, as the slope of the  $n$  vs  $U/2 - \mu$  curve is markedly steep. Eventually this seems to turn into a diverging charge compressibility, which is a typical signature of the onset of a phase transition [50]. In Figs. 1 and 2 the initial plateau of the occupations

TABLE I. Eigenstates of the isolated dimer Hamiltonian in the Dimer and  $B/A$  basis and their respective quantum numbers is shown in this table.  $N$  indicates the number of particles,  $S$  the total spin,  $S_z$  the  $z$  component of the spin operator, and  $\epsilon_k$  the energy associated to the state.

No.	$N$	$S$	$S_z$	$\epsilon_k$	Dimer basis	$B/A$ basis
0	0	0	0	0	$ 0, 0\rangle$	$ 0, 0\rangle$
1	1	$\frac{1}{2}$	$-\frac{1}{2}$	$-t_\perp$	$\frac{ \downarrow, 0\rangle -  \uparrow, 0\rangle}{\sqrt{2}}$	$ \downarrow, 0\rangle$
2	1	$\frac{1}{2}$	$-\frac{1}{2}$	$t_\perp$	$\frac{ \downarrow, 0\rangle +  \uparrow, 0\rangle}{\sqrt{2}}$	$ 0, \downarrow\rangle$
3	1	$\frac{1}{2}$	$\frac{1}{2}$	$-t_\perp$	$\frac{ \uparrow, 0\rangle -  \downarrow, 0\rangle}{\sqrt{2}}$	$ \uparrow, 0\rangle$
4	1	$\frac{1}{2}$	$\frac{1}{2}$	$t_\perp$	$\frac{ \uparrow, 0\rangle +  \downarrow, 0\rangle}{\sqrt{2}}$	$ 0, \uparrow\rangle$
5	2	1	1	0	$ \uparrow, \uparrow\rangle$	$ \uparrow, \uparrow\rangle$
6	2	1	0	0	$\frac{ \uparrow, \downarrow\rangle +  \downarrow, \uparrow\rangle}{\sqrt{2}}$	$\frac{ \uparrow, \downarrow\rangle +  \downarrow, \uparrow\rangle}{\sqrt{2}}$
7	2	0	0	$U$	$\frac{ \uparrow, \downarrow, 0\rangle -  \downarrow, \uparrow, 0\rangle}{\sqrt{2}}$	$\frac{ \downarrow, \uparrow\rangle -  \uparrow, \downarrow\rangle}{\sqrt{2}}$
8	2	0	0	$e_-$	$\frac{-\sigma_1( \uparrow, \downarrow\rangle +  \downarrow, \uparrow\rangle) +  \uparrow, \downarrow, 0\rangle +  \downarrow, \uparrow, 0\rangle}{\sqrt{2+2\sigma_1^2}}$	$c \uparrow, \downarrow, 0\rangle - s 0, \uparrow, \downarrow\rangle$
9	2	0	0	$e_+$	$\frac{\sigma_2( \uparrow, \downarrow\rangle -  \downarrow, \uparrow\rangle) +  \uparrow, \downarrow, 0\rangle +  \downarrow, \uparrow, 0\rangle}{\sqrt{2+2\sigma_2^2}}$	$s \uparrow, \downarrow, 0\rangle + c 0, \uparrow, \downarrow\rangle$
10	2	1	-1	0	$ \downarrow, \downarrow\rangle$	$ \downarrow, \downarrow\rangle$
11	3	0.5	-0.5	$U - t_\perp$	$\frac{ \uparrow, \downarrow, \downarrow\rangle +  \downarrow, \uparrow, \downarrow\rangle}{\sqrt{2}}$	$ \uparrow, \downarrow, \downarrow\rangle$
12	3	0.5	-0.5	$U + t_\perp$	$\frac{ \uparrow, \downarrow, \downarrow\rangle -  \downarrow, \uparrow, \downarrow\rangle}{\sqrt{2}}$	$ \downarrow, \uparrow, \downarrow\rangle$
13	3	0.5	0.5	$U - t_\perp$	$\frac{ \uparrow, \downarrow, \uparrow\rangle +  \downarrow, \uparrow, \uparrow\rangle}{\sqrt{2}}$	$ \uparrow, \downarrow, \uparrow\rangle$
14	3	0.5	0.5	$U + t_\perp$	$\frac{ \uparrow, \downarrow, \uparrow\rangle -  \downarrow, \uparrow, \uparrow\rangle}{\sqrt{2}}$	$ \uparrow, \downarrow, \uparrow\rangle$
15	4	0	0	$2U$	$ \uparrow, \downarrow, \uparrow, \downarrow\rangle$	$ \uparrow, \downarrow, \uparrow, \downarrow\rangle$

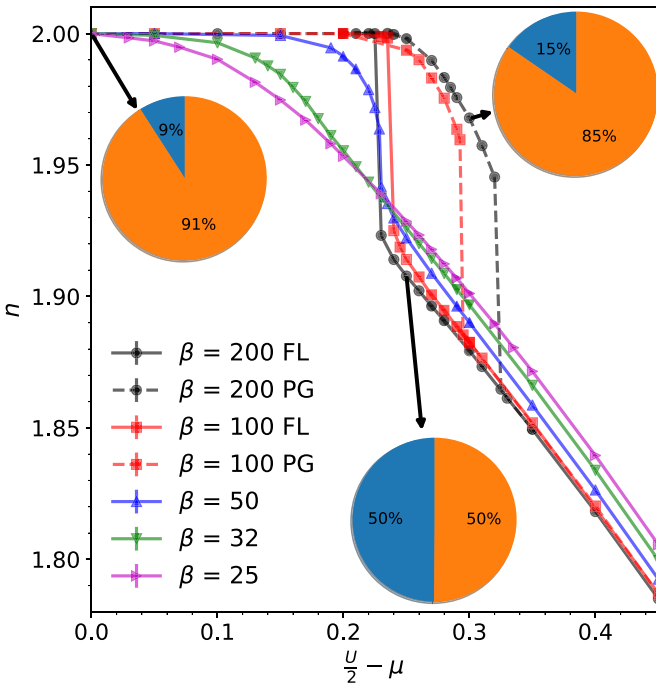


FIG. 1. The electron density  $n$  as a function of the renormalized chemical potential  $\frac{U}{2} - \mu$ . The half filling corresponds to  $n = 2$ , where the system is a Mott insulator. The hysteresis behavior above  $\beta = 50$  defines a PG-metal-to-metal coexistence region. Note the enhancement of the compressibility at the end point of the first-order transition (blue line) at  $\beta = 50$ . The orange sector of the pie charts indicates the relative contribution of the singlet states to the DAIM wave function projected on the isolated dimer for selected results at  $\beta = 200$ . The blue sector corresponds to all other states (see details in Table I).

testifies to the incompressible Mott insulator state. At higher  $\mu$ , the total and bond's occupations decrease continuously while the antibond's one increases. After this crossover this PG state at low temperature goes through a coexisting region with a FL solution. Such hysteretical behavior is the trademark of a first-order transition after which all occupations decrease uniformly, as shown in Fig. 2. At  $\beta = 50$  the occupation is continuous and the charge compressibility of the bond has a positive peak indicating a second-order critical point at lower temperature. Meanwhile the one of the antibond has a peak of smaller magnitude and opposite sign indicating a phase separation that evolves in a compressible metallic state at greater chemical potential. Indeed, by further reducing temperature ( $T = 1/\beta < 1/50$ ) we obtain a coexistence region between two distinct metallic states, one continuously connected to the insulator and the other continuously connected to the high doping metal. We shall show that the former is a PG metal while the latter is a conventional FL with quasiparticles, which characterize this first-order metal-to-metal transition. To gain insight into the nature of these two qualitatively different metallic phases, we display in Figs. 3(a) and 3(b) the imaginary part of the dimer Green's function,  $G_{B/AB}(\omega_1)$ , which directly outputs from the CTQMC-DMFT, evaluated at the first Matsubara frequency  $\omega_1$ , as a function of temperature. This is a useful quantity as it is a measure of the spectral intensity at low frequency. Moreover, for  $T \rightarrow 0$  it approaches the density of states at the Fermi energy  $D(E_F)$ , thus providing a convenient criterion to distinguish metal from insulator states. A conventional FL metal is characterized by the presence of a quasiparticle spectral weight at the Fermi level. Indeed, at doping  $n = 1.91$  (blue-diamond line), we observe that both  $\text{Im}G_{B/AB}(\omega_1)$  approach a similar finite value for  $T \rightarrow 0$ . The

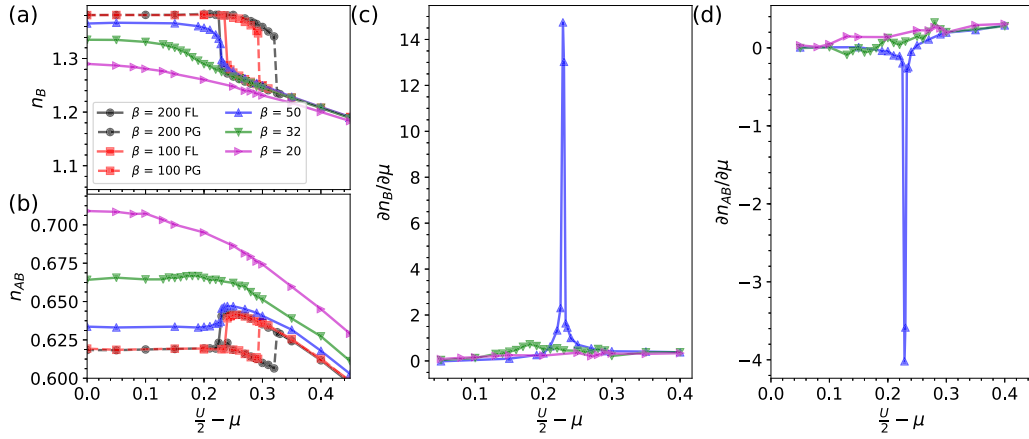


FIG. 2. (a, b) Occupation of the bond and of the antibond band. (d, e) Their charge compressibility.

high doping phase is therefore a normal correlated FL. In contrast, in the insulating phase at half filling  $n = 2$  (black-bullet line), the low frequency spectral weight gets depleted [ $\text{Im}G(\omega_1) \rightarrow 0$  as  $T \rightarrow 0$ ] as the Mott gap opens.

The interesting behavior appears for  $n = 1.97$  (red-square line) in the low doping metallic phase. While the  $B$  contribution displays metallic behavior as  $G_B(\omega_1)$  extrapolates to a finite value for  $T \rightarrow 0$ , the  $AB$  contribution, in contrast, loses spectral intensity at low frequency. Indeed,  $\text{Im}G_{AB}(\omega_1)$  extrapolates to zero, or to a small finite value, when  $T \rightarrow 0$ . This anomalous state is an instance of orbital selectivity, which is related to the findings made with the valence-bond DMFT [51–53].

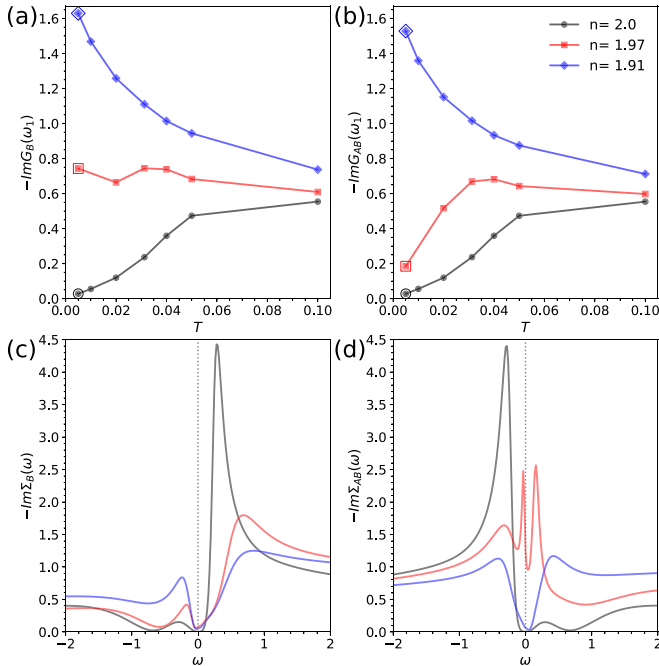


FIG. 3. (a, b)  $-\text{Im}G_B(\omega_1)$  and  $-\text{Im}G_{AB}(\omega_1)$  as a function of  $T$  for densities  $n = 2.0, 1.97, 1.91$ , where  $\omega_1$  is the first Matsubara frequency. (c, d)  $-\text{Im}\Sigma_B(\omega)$  and  $-\text{Im}\Sigma_{AB}(\omega)$  as a function of real frequency  $\omega$  for the same densities and the lowest temperature  $T = 1/\beta = 0.005$ .

To better understand the physical meaning of these results, it is useful to display on the real axis the imaginary part of the corresponding self-energy  $\Sigma_{B/AB}(\omega) = \mathcal{G}_{oB/AB}^{-1}(\omega) - G_{B/AB}^{-1}(\omega)$ . The analytical continuation to the real axis of the CTQMC was obtained with a standard maximum entropy method. The self-energies are a measure of the correlation contribution to the many-body system and reveal the qualitatively different nature of the metallic states [see Figs. 3(c) and 3(d)]. We can first discuss the more conventional Mott insulator and FL phases at  $n = 2.0$  and  $1.91$ , respectively. Similarly to the familiar case of the single-site Mott insulator, where the correlation gap opens due to a pole in  $\Sigma(\omega = 0)$ , in the DHM the Mott gap opens by the same mechanism, but with a small difference. While in the single-site case the Mott localized electrons are independent and incoherent spin  $1/2$ , here they are in dimers and form a liquid of singlets (see Fig. 1). The intradimer hopping then splits the central pole symmetrically in  $\Sigma_{B/AB}$  at  $\omega = \pm t_{\text{perp}}$ , as, respectively, seen in Figs. 3(c) and 3(d) [8,42].

Upon doping, the peak feature is strongly reduced, the Mott gap closes, and the relevant energy scale is close to  $\omega = 0$ . In a metal, the FL prescription requires that  $\text{Im}\Sigma \sim \omega^2$ . This behavior is observed in the FL phase ( $n = 1.91$  blue line), in  $\text{Im}\Sigma_{B/AB}$ , in agreement with the behavior of  $\text{Im}G_{AB}$  discussed in Figs. 3(a) and 3(b). On the other hand, in the PG metal ( $n = 1.97$  red line), while  $\text{Im}\Sigma_B$  still displays a FL behavior at low frequency,  $\text{Im}\Sigma_{AB}$  completely breaks the FL, displaying a peaklike behavior at  $\omega = 0$ , reminiscent of previous results on a slightly doped Mott-Hubbard insulator in two dimensions [52,54].

The PG metal appears to be smoothly connected to the Mott insulating state, as shown by the smooth evolution of the plateau in  $n$  vs  $\mu$  seen in Fig. 1 [28]. The origin of the PG insulating component can be traced back to the Mott insulating state, which in the DHM is sharply distinct from the paramagnetic Mott insulator of single-site DMFT [8,42]. In the DHM the physical properties are dominated by singlet formation via correlation enhancement of the intradimer hopping  $t_{\perp}$  (through  $\Sigma_{12}$ ) [8]. Two magnetic screening mechanisms are thus in competition: on one hand, the boosted intersite antiferromagnetic exchange interaction that tends to create singlets and an insulator, and, on the other, the on-site Kondo effect by



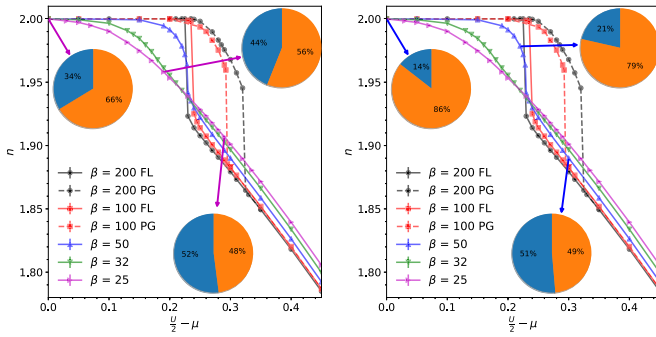


FIG. 4. The electron density  $n$  as a function of the renormalized chemical potential  $\frac{U}{2} - \mu$ . The half filling corresponds to  $n = 2$ , where the system is a Mott insulator. The hysteresis behavior above  $\beta = 50$  defines a PG-metal-to-metal coexistence region. Note the enhancement of the compressibility at the end point of the first-order transition (blue line) at  $\beta = 50$ . The orange sector of the pie charts indicates the relative contribution of the singlet states to the DAIM wave function projected on the isolated dimer for selected results on the left panel at  $\beta = 50$  and on the right panel at  $\beta = 25$ . The blue sector corresponds to all other states.

the environment electrons acting independently at each of the two sites of the dimer and favoring a metallic state. To show this connection, in Fig. 1 we display pie charts showing in orange the singlet contribution to the wave-function projection on the dimer sites (Table I). The blue sector corresponds to the participation of all the other states. In the Mott insulator the singlet contribution is 91%, and it is still a largely majoritarian 85% in the PG phase, once holes are introduced into the systems. This must be contrasted with the FL phase, where the singlet appear to have a 50% contribution, comparable with that of other components. In Fig. 4 we exhibit the behavior of the evolution of pie charts with temperature. The PG phase can be qualitatively viewed as a soup of singlets and strongly damped [as described by  $-\text{Im}\Sigma_B(\omega)$  in Fig. 3(c)] FL-like hole carriers. The PG phase that we established here within the DHM bears strong resemblance with the bad metal phase found in the context of many correlated materials, like in the organic salts, heavy fermions, iron-based superconductors, and, in particular, the cuprate high temperature superconductors. More generally, this phase appears as the natural outcome when one goes beyond the single-site approximations intrinsic to DMFT in infinite dimensions, in analogy with the “orbital selective” Mott transition of multiorbital correlated systems [35,55–59].

We argued above that the DHM PG metal exhibits orbital selectivity. We shall now show that, interestingly, that state bears resemblance to the results from cluster extensions of the Hubbard model in two dimensions [29,30,60], where the PG state was argued to emerge from a “momentum-selective” Mott transition [52,61–64]. This can be seen from the  $\epsilon$ -resolved spectral functions  $A(\omega, \epsilon)$ , where single particle energy  $\epsilon$  plays a similar role as the lattice momentum [24], since  $A_{B/AB}(\omega, \epsilon) = -\text{Im}\{1/[\omega + \mu - \epsilon - \Sigma_{B/AB}(\omega)]\}$ . The results are shown in Fig. 5, which we obtain by analytic continuation. At small doping ( $n = 1.97$ ), we obtain the PG-metal solution. In the  $B$  component [Figs. 5(a) and 5(b)], a coherent and dispersive narrow band appears at the Fermi level, which

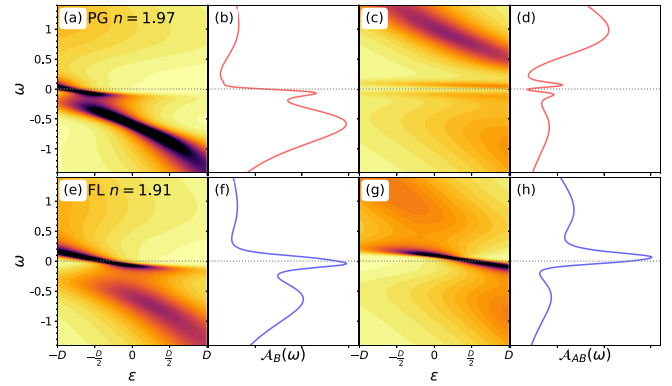


FIG. 5. Electronic dispersion  $A_{B/AB}(\omega, \epsilon)$  and local density of states  $A_{B/AB}(\omega) = \int d\epsilon A_{B/AB}(\omega, \epsilon)$  ( $B$  first and second column and  $AB$  third and fourth). The top line has the PG metal and the bottom line the FL metal.

produces a narrow FL peak in the respective DOS. In stark contrast, the  $AB$  component [Figs. 5(c) and 5(d)] develops two parallel and weakly dispersive features around the Fermi level, which produce the PG-like dip in the DOS. Therefore, the PG metal possesses at the same time FL and non-FL character, qualitatively similar to the cluster extension and reminiscent of the physics of cuprates. On the other hand, at higher doping ( $n = 1.91$ ), the orbital selectivity disappears at low frequency. Both components [Figs. 5(e)–5(h)] display similarly dispersive coherent quasiparticle bands and quasiparticle peaks in the respective DOS, as expected in a conventional FL.

Finally, we obtained the optical conductivity that we show in Fig. 6 for the Mott insulator along with the PG- and the FL-metal states [8]. The Mott insulator has as expected a wide gap (black line  $n = 2$ ). In contrast, at high doping (blue line

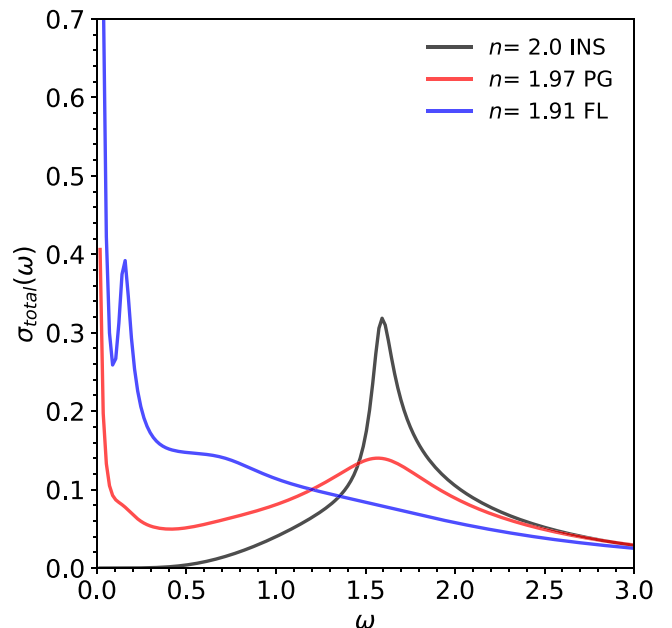


FIG. 6. Optical conductivity in the insulating phase ( $n = 2.0$ ) in black, PG phase ( $n = 1.97$ ) in red, and FL phase ( $n = 1.91$ ) in blue.

$n = 1.91$ ) the optical response, as expected in a correlated metal with quasiparticles, has a narrow Drude peak at low frequency, the spectral intensity of which denotes the effective carrier density. In addition, there is a midinfrared contribution ( $\omega \sim 0.2$ ) that has been previously identified as originated in the intradimer hopping [8]. Interestingly, in between these two states we find the optical response of the PG metal (red line  $n = 1.97$ ), which combines features of both. At low frequency, it shows a narrow and relatively small Drude peak that can be traced to the FL metal of the  $B$  component. This contribution coexists with a midinfrared contribution that lost a significant amount of spectral intensity and is associated to the incoherent PG state realized in the  $AB$  component. It is interesting to note that this optical conductivity response bears some resemblance with the one observed in the PG phase of cuprates [65,66].

### III. DISCUSSION

To conclude, we obtained the numerical quantum Monte Carlo solution on the dimer Hubbard model within DMFT, which is the exact solution of the model in the limit of large dimensions. This model is arguably the minimal Hubbard-like model that embodies on equal footing on-site correlations and nonlocal magnetic interactions. Our main result was to establish the existence of the doping-driven first-order metal-to-metal transition between a pseudogap metal and a Fermi

liquid one. It is interesting to mention an exciting consequence of our paper, which may be experimentally explored, namely, that one may turn the first-order metal-insulator transition of  $\text{VO}_2$  into a metal-metal one by electrostatic gating of a  $\text{VO}_2$  thin film. In such a case, the transition would be between the conventional rutile metal and a metallic PG state. Moreover, it is tempting to speculate that such a state may be the *monoclinic metal*, which has been reported in multiple studies of  $\text{VO}_2$  [7,67,68]. From a wider theoretical perspective, our paper helps to clarify an important on-going debate. It provides a concrete realization, with an explicit rationale, for the origin of several unconventional properties such as bad metal behavior, the pseudogap, orbital selective Mott transitions, and enhanced compressibilities [35,38,62–64,69,70], which are relevant to doped Mott insulators and correlated quantum materials in general [71–73].

### ACKNOWLEDGMENTS

S.B., M.C., and M.R. acknowledge support from French ANR “MoMA” Project No. ANR-19-CE30-0020. L.F. is supported by the UCSD-CNRS collaboration Quantum Materials for Energy Efficient Neuromorphic Computing, an Energy Frontier Research Center funded by the U.S. Department of Energy, Office of Science, Basic Energy Sciences under Grant No. DE-SC0019273. A.C. is supported by CONICET, AN-CyT, and UBACyT, Argentina.

- 
- [1] M. Imada, A. Fujimori, and Y. Tokura, Metal-insulator transitions, *Rev. Mod. Phys.* **70**, 1039 (1998).
  - [2] C. Proust and L. Taillefer, The remarkable underlying ground states of cuprate superconductors, *Annu. Rev. Condens. Matter Phys.* **10**, 409 (2019).
  - [3] E. Dagotto, *Nanoscale Phase Separation and Colossal Magnetoresistance: The Physics of Manganites and Related Compounds* (Springer-Verlag, Berlin, 2003).
  - [4] J. del Valle, J. G. Ramirez, M. J. Rozenberg, and I. K. Schuller, Challenges in materials and devices for resistive-switching-based neuromorphic computing, *J. Appl. Phys.* **124**, 211101 (2018).
  - [5] N. F. Mott, Metal-Insulator Transition, *Rev. Mod. Phys.* **40**, 677 (1968).
  - [6] Z. Yang, C. Ko, and S. Ramanathan, Oxide electronics utilizing ultrafast metal-insulator transitions, *Annu. Rev. Mater. Res.* **41**, 337 (2011).
  - [7] M. M. Qazilbash, M. Brehm, B.-G. Chae, P.-C. Ho, G. O. Andreev, B.-J. Kim, S. J. Yun, A. V. Balatsky, M. B. Maple, F. Keilmann, H.-T. Kim, and D. N. Basov, Mott transition in  $\text{VO}_2$  revealed by infrared spectroscopy and nano-imaging, *Science* **318**, 1750 (2007).
  - [8] O. Nájera, M. Civelli, V. Dobrosavljevic, and M. J. Rozenberg, Resolving the  $\text{VO}_2$  controversy: Mott mechanism dominates the insulator-to-metal transition, *Phys. Rev. B* **95**, 035113 (2017).
  - [9] H. T. Stinson, A. Sternbach, O. Najera, R. Jing, A. S. Mcleod, T. V. Slusar, A. Mueller, L. Andereg, H. T. Kim, M. Rozenberg, and D. N. Basov, Imaging the nanoscale phase separation in vanadium dioxide thin films at terahertz frequencies, *Nat. Commun.* **9**, 3604 (2018).
  - [10] K. Shibuya, M. Kawasaki, and Y. Tokura, Metal-insulator transition in epitaxial  $\text{VO}_2$  thin films, *Appl. Phys. Lett.* **96**, 022102 (2010).
  - [11] X. Tan, T. Yao, R. Long, Z. Sun, Y. Feng, H. Cheng, X. Yuan, W. Zhang, Q. Liu, C. Wu, Y. Xie, and S. Wei, Unraveling metal-insulator transition mechanism of  $\text{VO}_2$  triggered by tungsten doping, *Sci. Rep.* **2**, 466 (2012).
  - [12] J. Jeong, N. Aetukuri, T. Graf, T. D. Schladt, M. G. Samant, and S. S. P. Parkin, Suppression of metal-insulator transition in  $\text{VO}_2$  by electric field induced oxygen vacancy formation, *Science* **339**, 1402 (2013).
  - [13] T. Yajima, T. Nishimura, and A. Toriumi, Positive-bias gate-controlled metal-insulator transition in ultrathin  $\text{VO}_2$  channels with  $\text{TiO}_2$  gate dielectrics, *Nat. Commun.* **6**, 10104 (2015).
  - [14] Y. Kalcheim, A. Camjayi, J. del Valle, P. Salev, M. Rozenberg, and I. K. Schuller, Non-thermal resistive switching in Mott insulator nanowires, *Nat. Commun.* **11**, 2985 (2020).
  - [15] W. Yi, K. K. Tsang, S. K. Lam, X. Bai, J. A. Crowell, and E. A. Flores, Biological plausibility and stochasticity in scalable  $\text{VO}_2$  active memristor neurons, *Nat. Commun.* **9**, 4661 (2018).
  - [16] J. del Valle, P. Salev, F. Tesler, N. M. Vargas, Y. Kalcheim, P. Wang, J. Trastoy, M.-H. Lee, G. Kassabian, J. G. Ramírez, M. J. Rozenberg, and I. K. Schuller, Subthreshold firing in Mott nanodevices, *Nature (London)* **569**, 388 (2019).
  - [17] J. del Valle, N. M. Vargas, R. Rocco, P. Salev, Y. Kalcheim, P. N. Lapa, C. Adda, M.-H. Lee, P. Y. Wang, L. Fratino, M. J. Rozenberg, and I. K. Schuller, Spatiotemporal characterization of the field-induced insulator-to-metal transition, *Science* **373**, 907 (2021).

- [18] S. Biermann, A. Poteryaev, A. I. Lichtenstein, and A. Georges, Dynamical Singlets and Correlation-Assisted Peierls Transition in  $\text{VO}_2$ , *Phys. Rev. Lett.* **94**, 026404 (2005).
- [19] J. M. Tomczak, F. Aryasetiawan, and S. Biermann, Effective bandstructure in the insulating phase versus strong dynamical correlations in metallic  $\text{VO}_2$ , *Phys. Rev. B* **78**, 115103 (2008).
- [20] C. Weber, D. D. O'Regan, N. D. M. Hine, M. C. Payne, G. Kotliar, and P. B. Littlewood, Vanadium Dioxide: A Peierls-Mott Insulator Stable against Disorder, *Phys. Rev. Lett.* **108**, 256402 (2012).
- [21] W. H. Brito, M. C. O. Aguiar, K. Haule, and G. Kotliar, Metal-Insulator Transition in  $\text{VO}_2$ : A DFT + DMFT Perspective, *Phys. Rev. Lett.* **117**, 056402 (2016).
- [22] S. Gazit, F. F. Assaad, and S. Sachdev, Fermi Surface Reconstruction without Symmetry Breaking, *Phys. Rev. X* **10**, 041057 (2020).
- [23] H. Shackleton, A. Wietek, A. Georges, and S. Sachdev, Quantum Phase Transition at Nonzero Doping in a Random  $t-J$  Model, *Phys. Rev. Lett.* **126**, 136602 (2021).
- [24] A. Georges, G. Kotliar, W. Krauth, and M. J. Rozenberg, Dynamical mean-field theory of strongly correlated fermion systems and the limit of infinite dimensions, *Rev. Mod. Phys.* **68**, 13 (1996).
- [25] Y. Núñez-Fernández, G. Kotliar, and K. Hallberg, Emergent low-energy bound states in the two-orbital Hubbard model, *Phys. Rev. B* **97**, 121113(R) (2018).
- [26] M. Harland, A. I. Poteryaev, S. V. Streltsov, and A. I. Lichtenstein, Electronic correlations and competing orders in multiorbital dimers: A cluster DMFT study, *Phys. Rev. B* **99**, 045115 (2019).
- [27] G. Kotliar and D. Vollhardt, Strongly correlated materials: Insights from dynamical mean-field theory, *Phys. Today* **57**(3), 53 (2004).
- [28] G. Sordi, K. Haule, and A.-M. S. Tremblay, Finite Doping Signatures of the Mott Transition in the Two-Dimensional Hubbard Model, *Phys. Rev. Lett.* **104**, 226402 (2010).
- [29] B. Kyung, S. S. Kancharla, D. Sénéchal, A.-M. S. Tremblay, M. Civelli, and G. Kotliar, Pseudogap induced by short-range spin correlations in a doped Mott insulator, *Phys. Rev. B* **73**, 165114 (2006).
- [30] A. Macridin, M. Jarrell, T. Maier, P. R. C. Kent, and E. D'Azevedo, Pseudogap and Antiferromagnetic Correlations in the Hubbard Model, *Phys. Rev. Lett.* **97**, 036401 (2006).
- [31] E. Gull, M. Ferrero, O. Parcollet, A. Georges, and A. J. Millis, Momentum-space anisotropy and pseudogaps: A comparative cluster dynamical mean-field analysis of the doping-driven metal-insulator transition in the two-dimensional Hubbard model, *Phys. Rev. B* **82**, 155101 (2010).
- [32] E. Gull, O. Parcollet, and A. J. Millis, Superconductivity and the Pseudogap in the Two-Dimensional Hubbard Model, *Phys. Rev. Lett.* **110**, 216405 (2013).
- [33] S. Sakai, Y. Motome, and M. Imada, Evolution of Electronic Structure of Doped Mott Insulators: Reconstruction of Poles and Zeros of Green's Function, *Phys. Rev. Lett.* **102**, 056404 (2009).
- [34] A. Liebsch and N.-H. Tong, Finite-temperature exact diagonalization cluster dynamical mean-field study of the two-dimensional Hubbard model: Pseudogap, non-Fermi-liquid behavior, and particle-hole asymmetry, *Phys. Rev. B* **80**, 165126 (2009).
- [35] L. de' Medici, A. Georges, and S. Biermann, Orbital-selective Mott transition in multiband systems: Slave-spin representation and dynamical mean-field theory, *Phys. Rev. B* **72**, 205124 (2005).
- [36] L. De Leo, M. Civelli, and G. Kotliar,  $T = 0$  Heavy-Fermion Quantum Critical Point as an Orbital-Selective Mott Transition, *Phys. Rev. Lett.* **101**, 256404 (2008).
- [37] V. I. Anisimov, I. A. Nekrasov, D. E. Kondakov, T. M. Rice, and M. Sigrist, Orbital-selective Mott-insulator transition in  $\text{Ca}_{2-x}\text{Sr}_x\text{RuO}_4$ , *Eur. Phys. J. B* **25**, 191 (2002).
- [38] L. de' Medici, S. R. Hassan, M. Capone, and X. Dai, Orbital-Selective Mott Transition out of Band Degeneracy Lifting, *Phys. Rev. Lett.* **102**, 126401 (2009).
- [39] P. Werner, E. Gull, and A. J. Millis, Metal-insulator phase diagram and orbital selectivity in three-orbital models with rotationally invariant Hund coupling, *Phys. Rev. B* **79**, 115119 (2009).
- [40] F. B. Kugler, S.-S. B. Lee, A. Weichselbaum, G. Kotliar, and J. von Delft, Orbital differentiation in Hund metals, *Phys. Rev. B* **100**, 115159 (2019).
- [41] B. Keimer, S. A. Kivelson, M. R. Norman, S. Uchida, and J. Zaanen, From quantum matter to high-temperature superconductivity in copper oxides, *Nature (London)* **518**, 179 (2015).
- [42] O. Nájera, M. Civelli, V. Dobrosavljević, and M. J. Rozenberg, Multiple crossovers and coherent states in a Mott-Peierls insulator, *Phys. Rev. B* **97**, 045108 (2018).
- [43] A. Georges, Strongly correlated electron materials: Dynamical mean-field theory and electronic structure, *arXiv:cond-mat/0403123* (2004).
- [44] G. Moeller, V. Dobrosavljević, and A. E. Ruckenstein, RKKY interactions and the Mott transition, *Phys. Rev. B* **59**, 6846 (1999).
- [45] A. Fuhrmann, D. Heilmann, and H. Monien, From Mott insulator to band insulator: A dynamical mean-field theory study, *Phys. Rev. B* **73**, 245118 (2006).
- [46] S. S. Kancharla and S. Okamoto, Band insulator to Mott insulator transition in a bilayer Hubbard model, *Phys. Rev. B* **75**, 193103 (2007).
- [47] H. Hafermann, M. Katsnelson, and A. Lichtenstein, Metal-insulator transition by suppression of spin fluctuations, *Europhys. Lett.* **85**, 37006 (2009).
- [48] E. Gull, A. J. Millis, A. I. Lichtenstein, A. N. Rubtsov, M. Troyer, and P. Werner, Continuous-time Monte Carlo methods for quantum impurity models, *Rev. Mod. Phys.* **83**, 349 (2011).
- [49] K. Haule, Quantum Monte Carlo impurity solver for cluster dynamical mean-field theory and electronic structure calculations with adjustable cluster base, *Phys. Rev. B* **75**, 155113 (2007).
- [50] G. Kotliar, S. Murthy, and M. J. Rozenberg, Compressibility Divergence and the Finite Temperature Mott Transition, *Phys. Rev. Lett.* **89**, 046401 (2002).
- [51] M. Ferrero, P. S. Cornaglia, L. De Leo, O. Parcollet, G. Kotliar, and A. Georges, Valence bond dynamical mean-field theory of doped Mott insulators with nodal/antinodal differentiation, *Europhys. Lett.* **85**, 57009 (2009).
- [52] M. Ferrero, P. S. Cornaglia, L. De Leo, O. Parcollet, G. Kotliar, and A. Georges, Pseudogap opening and formation of Fermi arcs as an orbital-selective Mott transition in momentum space, *Phys. Rev. B* **80**, 064501 (2009).



- [53] M. Ferrero, O. Parcollet, A. Georges, G. Kotliar, and D. N. Basov, Interplane charge dynamics in a valence-bond dynamical mean-field theory of cuprate superconductors, *Phys. Rev. B* **82**, 054502 (2010).
- [54] H. Bragança, S. Sakai, M. C. O. Aguiar, and M. Civelli, Correlation-Driven Lifshitz Transition at the Emergence of the Pseudogap Phase in the Two-Dimensional Hubbard Model, *Phys. Rev. Lett.* **120**, 067002 (2018).
- [55] Z. Yin, K. Haule, and G. Kotliar, Kinetic frustration and the nature of the magnetic and paramagnetic states in iron pnictides and iron chalcogenides, *Nat. Mater.* **10**, 932 (2011).
- [56] H. Ishida and A. Liebsch, Fermi-liquid, non-Fermi-liquid, and Mott phases in iron pnictides and cuprates, *Phys. Rev. B* **81**, 054513 (2010).
- [57] P. Werner, M. Casula, T. Miyake, F. Aryasetiawan, A. J. Millis, and S. Biermann, Satellites and large doping and temperature dependence of electronic properties in hole-doped BaFe<sub>2</sub>As<sub>2</sub>, *Nat. Phys.* **8**, 331 (2012).
- [58] S. Backes, H. O. Jeschke, and R. Valentí, Microscopic nature of correlations in multiorbital AFe<sub>2</sub>As<sub>2</sub> (A = K, Rb, Cs): Hund's coupling versus Coulomb repulsion, *Phys. Rev. B* **92**, 195128 (2015).
- [59] P. Werner, E. Gull, M. Troyer, and A. J. Millis, Spin Freezing Transition and Non-Fermi-Liquid Self-Energy in a Three-Orbital Model, *Phys. Rev. Lett.* **101**, 166405 (2008).
- [60] M. Civelli, M. Capone, S. S. Kancharla, O. Parcollet, and G. Kotliar, Dynamical Breakup of the Fermi Surface in a Doped Mott Insulator, *Phys. Rev. Lett.* **95**, 106402 (2005).
- [61] E. Gull, O. Parcollet, P. Werner, and A. J. Millis, Momentum-sector-selective metal-insulator transition in the eight-site dynamical mean-field approximation to the Hubbard model in two dimensions, *Phys. Rev. B* **80**, 245102 (2009).
- [62] G. Sordi, K. Haule, and A.-M. S. Tremblay, Mott physics and first-order transition between two metals in the normal-state phase diagram of the two-dimensional Hubbard model, *Phys. Rev. B* **84**, 075161 (2011).
- [63] G. Sordi, P. Sémon, K. Haule, and A.-M. S. Tremblay, *C*-axis resistivity, pseudogap, superconductivity, and Widom line in doped Mott insulators, *Phys. Rev. B* **87**, 041101(R) (2013).
- [64] G. Sordi, P. Sémon, K. Haule, and A.-M. S. Tremblay, Pseudogap temperature as a Widom line in doped Mott insulators, *Sci. Rep.* **2**, 547 (2012).
- [65] D. N. Basov and T. Timusk, Electrodynamics of high-*T<sub>c</sub>* superconductors, *Rev. Mod. Phys.* **77**, 721 (2005).
- [66] S. L. Cooper, D. Reznik, A. Kotz, M. A. Karlow, R. Liu, M. V. Klein, W. C. Lee, J. Giapintzakis, D. M. Ginsberg, B. W. Veal, and A. P. Paulikas, Optical studies of the *a*-, *b*-, and *c*-axis charge dynamics in YBa<sub>2</sub>Cu<sub>3</sub>O<sub>6+x</sub>, *Phys. Rev. B* **47**, 8233 (1993).
- [67] J. Laverock, S. Kittiwatanakul, A. A. Zakharov, Y. R. Niu, B. Chen, S. A. Wolf, J. W. Lu, and K. E. Smith, Direct Observation of Decoupled Structural and Electronic Transitions and an Ambient Pressure Monocliniclike Metallic Phase of VO<sub>2</sub>, *Phys. Rev. Lett.* **113**, 216402 (2014).
- [68] E. Arcangeletti, L. Baldassarre, D. Di Castro, S. Lupi, L. Malavasi, C. Marini, A. Perucchi, and P. Postorino, Evidence of a Pressure-Induced Metallization Process in Monoclinic VO<sub>2</sub>, *Phys. Rev. Lett.* **98**, 196406 (2007).
- [69] L. Fratino, P. Sémon, G. Sordi, and A.-M. S. Tremblay, An organizing principle for two-dimensional strongly correlated superconductivity, *Sci. Rep.* **6**, 22715 (2016).
- [70] L. Fratino, P. Sémon, G. Sordi, and A.-M. S. Tremblay, Pseudogap and superconductivity in two-dimensional doped charge-transfer insulators, *Phys. Rev. B* **93**, 245147 (2016).
- [71] E. Fradkin, S. A. Kivelson, and J. M. Tranquada, Colloquium: Theory of intertwined orders in high temperature superconductors, *Rev. Mod. Phys.* **87**, 457 (2015).
- [72] K. B. Efetov, H. Meier, and C. Pépin, Pseudogap state near a quantum critical point, *Nat. Phys.* **9**, 442 (2013).
- [73] V. J. Emery, S. A. Kivelson, and H. Q. Lin, Phase Separation in the *t* - *j* Model, *Phys. Rev. Lett.* **64**, 475 (1990).